HELICOPTER HOVER CEILING IMPROVEMENT POSSIBILITIES AND ITS LIMITS WITH AN ELECTRIC TAIL-ROTOR

Rajesh Kallur-Krishnamoorthy (kallur@dhbw-ravensburg.de),
Philipp Krämer (kraemer@dhbw-ravensburg.de),
DHBW Ravensburg (Germany)

Abstract
For conventional helicopters with single main-rotor and fixed-speed tail-rotor whose hover ceiling is limited by the tail-rotor thrust, variable speed electric tail-rotors could potentially improve hover ceiling by operating at higher rotor speed. On the basis of a 2D-panel method code and transonic small disturbance theory for airfoil section coefficients, and blade-element and momentum (BEM) theory model, the tail-rotor performance is analysed for higher rotor speeds compared to base configuration. Results are presented for an example existing helicopter for hover out-of-ground effect (OGE) with maximum take-off weight (MTOW) conditions. The results confirm that compressibility effects at the tip-section is the major limitation for operating at higher rotor speeds. Combined with the thrust and power balance for the tail-rotor and helicopter powerplant respectively, hover ceiling improvement is quantified. In spite of the limited speed increase possibility due to compressibility effects a noticeable improvement to hover ceiling is made possible with the variable speed electric tail-rotor configuration.

1. INTRODUCTION

Most conventional helicopter tail-rotors are driven by long mechanical drive shafts and gearboxes at a fixed transmission ratio to the main-rotor speed. By replacing the mechanical tail-rotor power transmission with an electrical power transmission, potential benefits such as improved flight envelope characteristics, potential to reduce tail-rotor noise, reduced maintenance and the possibility to open up new helicopter design configurations may be realized. With flight envelope characteristics - specifically that of improved hover ceiling and improved available yaw margin are possible. Such benefits are mainly a result of the possibility to individually vary the electric motor speed as opposed to a conventional drive with fixed speed.

Some of these benefits to flight envelope improvement have also been briefly identified as part of a variable transmission drive train for rotors study with the proposal to operate at higher rotor speeds to improve hover ceiling[1]. Studies on variable speed main-rotors have also detailed discussions on the benefits in power savings with increasing advance ratio[2][3]. It is also well-known that reduced rotor noise can be achieved by means of reducing rotor speed[4], which could be a consideration for operation at lower altitudes. This opens up a possibility of using electric motor driven variable tail-rotors to cover possible speed variation based improvements. This paper aims to discuss in detail the case of an electric tail-rotor especially for hover in high altitude, which is a distinctive limitation on the helicopter's overall flight envelope, and to more precisely identify the limits of its application.

Two effects are main contributors for these limitations: a) total power balance equation (at the helicopter powerplant/main gearbox level) and b) compressibility effects at higher Mach number due to increased rotor tip-speed. Establishing these limits will help establish boundaries to the scope of improvement of helicopter hover ceiling, on the basis of an electric tail-rotor system layout.

2. METHODOLOGY

The tail-rotor aerodynamic performance estimates are generated as a function of tail-rotor collective pitch input, variable operational speed and altitude. The nature of the study being one of preliminary design, the calculation methods used are selected for speed and simplicity over complex computational methods. Results are discussed based on an example European helicopter, belonging to the upper

end of Category A, Small Rotorcraft classification under EASA CS-27 regulations, operating in hover OGE at maximum take-off weight (MTOW). Tail-rotor performance results with conventional fixed-speed configuration is compared against operating at higher tail-rotor speeds.

2.1 Rotor aerodynamic model

The study uses a parametric steady state rotor aerodynamic model based on the well-known Actuator Disk (AD) theory and Blade-Element and Momentum (BEM) theory[5]. The AD theory model is used to calculate the main-rotor torque on airframe that needs to be reacted for at MTOW condition. The BEM theory model is used for the tail-rotor performance calculation. The BEM theory model was implemented as MATLAB® code and an iterative solver for a non-linear equation was used. The rotor power and thrust coefficients per solidity are their commonly used definitions[5]. The BEM theory model has been validated against published data[6], depicted in Figure 1.

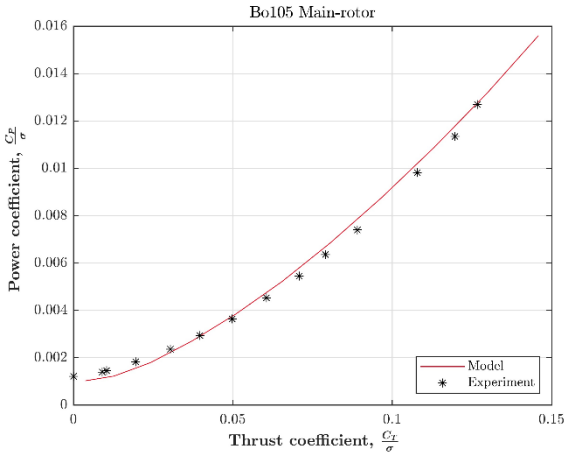

Figure 1 Rotor aerodynamic model based on BEM theory results compared to measured data of Bo105 Main-rotor in hover OGE

2.2 Airfoil section coefficients

2-Dimensional Airfoil section coefficients are obtained by means of a widely used 2-D panel method code, with a boundary layer model based on source distributions to model viscous effects[7]. The code also implements a Karman-Tsien compressibility correction in order to provide results at higher subsonic Mach numbers. Additionally, for flow conditions with upstream transonic conditions a code based on transonic small disturbance theory equations[8] is used to obtain the section wave drag coefficient, C_{dW}. The calculated coefficients were compared to selected measured data for NACA 0012 airfoil. Figure 2 shows the calculated lift-drag polar compared to subsonic measured data [9] and shows good agreement.

Figure 3 shows the calculated lift drag polar against transonic measured data[10]. Here there is good agreement of lift coefficient (C_l) values of up to 0.5 after which total drag coefficient (C_d) values are overestimated.

Figure 4 shows the zero-lift drag coefficient over Mach number including the large drag increase due to wave-drag rise around a Mach number of 0.77. Here too there is good agreement of calculated data with measured data[11]. For preliminary design purposes the major trends are shown and agreement of calculated data is deemed acceptable.

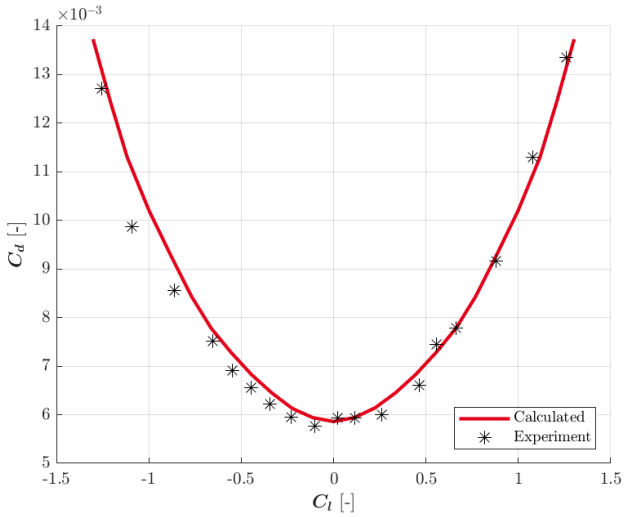

Figure 2 NACA 0012 Lift-drag polar for subsonic flow at Re=3x10^6 and free transition

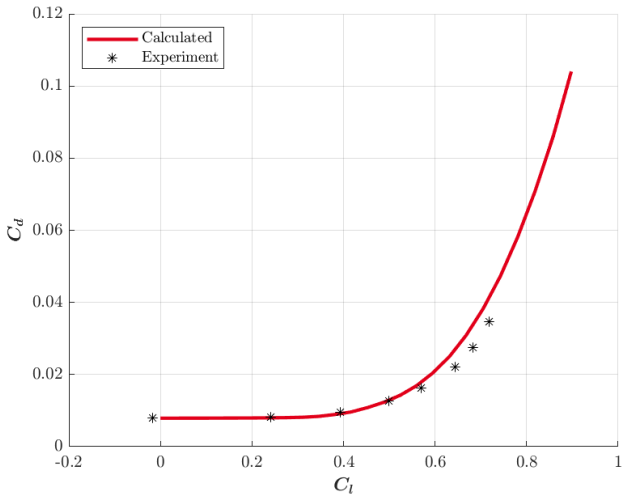

Figure 3 NACA 0012 Lift-drag polar with transonic flow conditions at M∞ = 0.7, Re = 9x10^6, forced transition at x/c=0.05

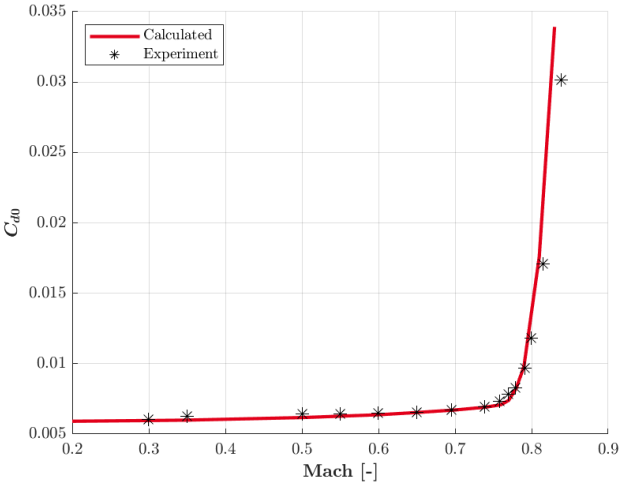

Figure 4 NACA 0012 zero-lift drag coefficient over Mach number with Re=3x10^6 and free transition

2.3 Compressibility effect limits

The study considers the limits due to compressibility effects for increased blade-tip Mach number when increasing rotor operational speed. To this end one of the two commonly accepted conventional definition of drag-divergence Mach number is used, namely the rise of wave drag coefficient (C_{dW}) up to a count of 20, i.e., $C_{dW} = 0.002$[12]–[14]. Above this value the wave drag rise is steep signifying stronger shock waves due to upstream transonic airflow. This effect can also be seen in Figure 4. For the NACA 0012 profile the drag divergence Mach number calculated is at 0.79.

2.4 Tail-rotor configuration

The base configuration tail-rotor is the conventional tail-rotor system that operates at the design fixed-speed, N_{ref} and is able to produce varying levels of thrust by varying the blade pitch angle by means of its collective pitch input. The study considers the possibility of free variation of rotor operational speed by means of an electric rotor drive replacing the tail-rotor drive shaft and gearbox. In addition to the conventional blade pitch variation the variation of speed also varies thrust output. All other parameters such as rotor dimensions, airfoil profile, chord, number of blades and blade twist are all unaltered compared to the base tail-rotor. For simplicity, the rotor is in isolation and no main-rotor tail-rotor interference is considered. Moreover, the analysis is for hover OGE conditions with zero crosswind. The main-rotor is assumed to be a conventional fixed speed system.

The airfoil considered for the tail rotor of the chosen example helicopter is NACA 0012. The chosen example helicopter has a MTOW of 2900 kg. Steady-state tail-rotor thrust output is evaluated by the code for a given tail-rotor collective pitch input angle, operating at a designated steady state speed at a given altitude for the International Standard Atmosphere (ISA) conditions.

2.5 Powerplant output reduction over altitude

At higher operating altitudes turboshaft powerplants that are typically used in helicopters as chosen for this study have reduced power output. This is modelled by a highly simplified empirical relationship from literature[15],

$$P_h = P_0 \left(\frac{\rho_h}{\rho_0}\right)^{0.75} \quad (1)$$

Where P_0 and ρ_0 are the mean sea level (MSL) or reference power output and air density, P_h and ρ_h are the power output and air density at any given altitude for ISA conditions.

3. RESULTS AND DISCUSSION

The range of evaluated pitch input angles, rotor speeds and altitude are summarized in Table 1. The rotor speed of the base configuration with fixed-speed operation is taken to be the reference speed, N_{ref}.

Table 1 Range of evaluated tail-rotor operating points

Parameter	Minimum	Maximum	Units
Collective pitch input	0	34	deg
Rotor speed	100	115	%
Altitude	0	2600	m

Figure 5 shows a summary of performance for the altitude, $H = 0\,m$ (representing MSL) for different rotor operating speeds and over the entire range of collective pitch input. With increasing speed stall occurs at progressively earlier collective pitch input angle. This is because maximum C_l for the airfoil occurs at progressively lower angle of attack (α) for increasing Mach number as is common knowledge for NACA 0012[11][16]. The peak thrust achieved before stall for the base configuration (fixed speed N_{ref}) is taken as the reference tail-rotor thrust, T_{ref} and the corresponding power value as the reference tail-rotor power, P_{ref} in this study. For higher rotor operating speeds, the increase in thrust production comes at a higher power penalty. This is most evident when comparing with rotor power coefficients.

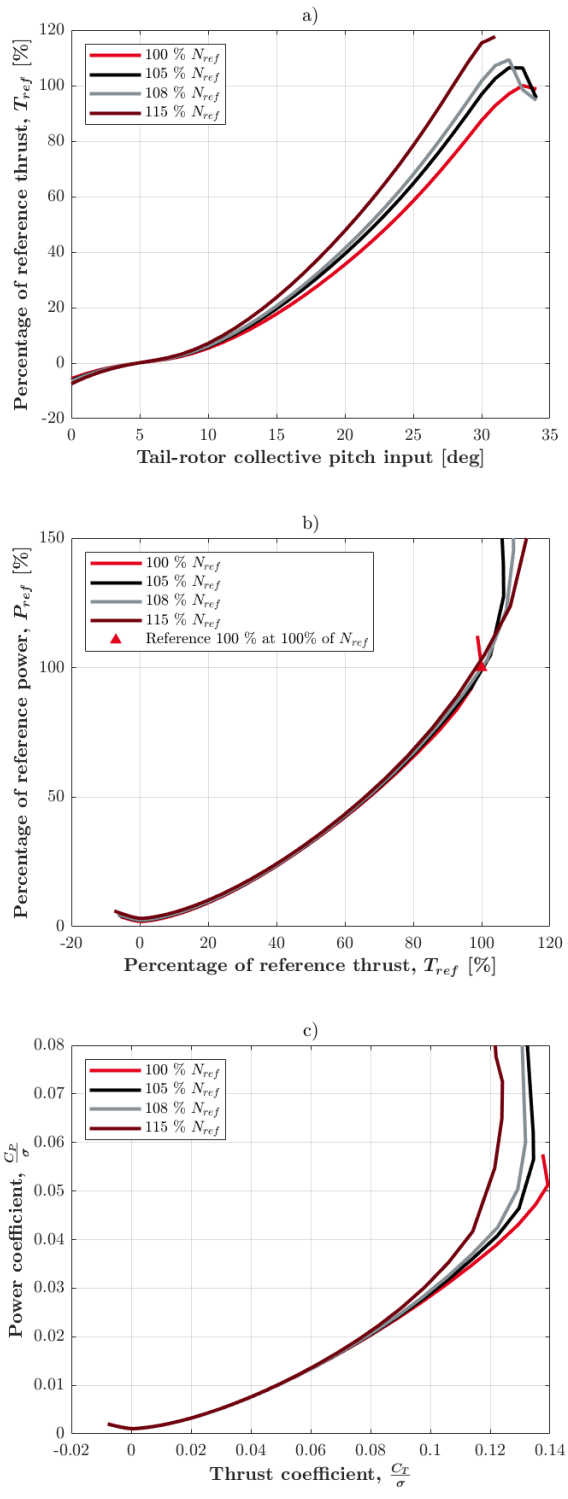

Figure 5 Tail-rotor performance figures for altitude H = 0 m, a) Thrust output over collective pitch input, b) Power required for Thrust output c) Power vs Thrust coefficient.

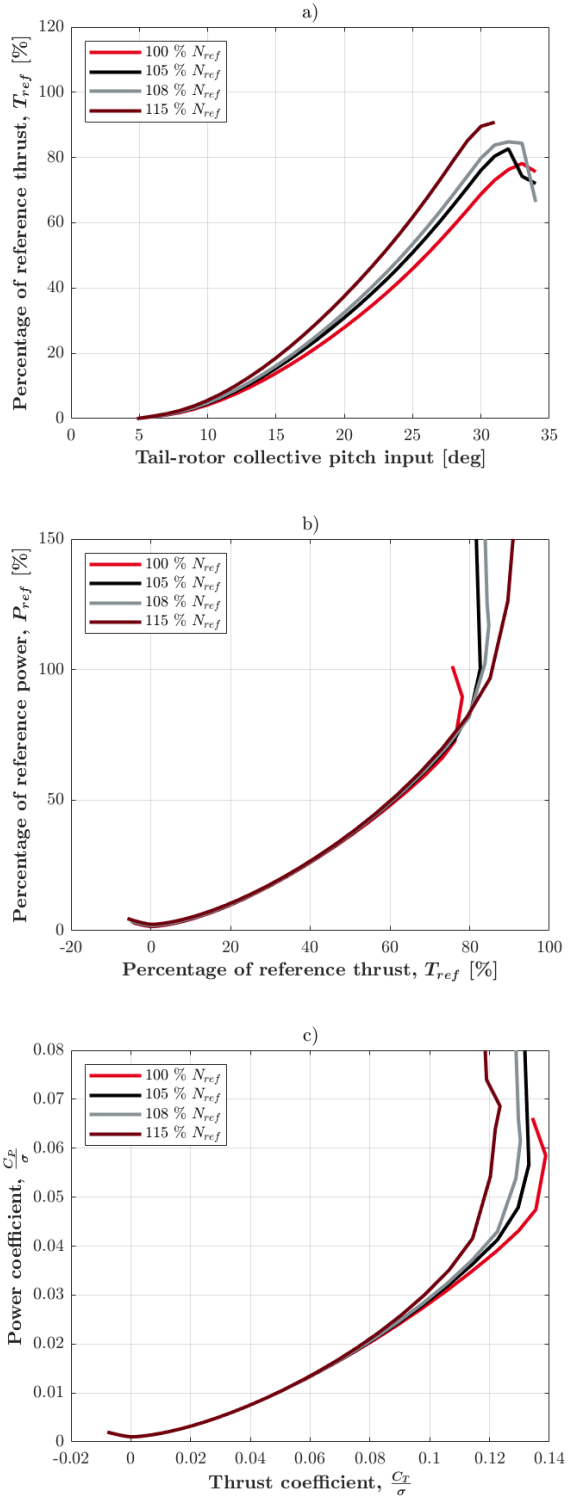

Figure 6 Tail-rotor performance figures for altitude H = 2000 m, a) Thrust output over collective pitch input, b) Power required for Thrust output c) Power vs Thrust coefficient.

Figure 6 shows the same for a representative hover altitude of 2000 m above MSL. Here too the effect of increasing the rotor speed has a large increase in power required.

The large increase in power with increased rotor speeds comes due to the blade tip section operating close or above the conventional definition of

compressibility limits as established earlier. Both the compressibility limit and the blade stall limit (C_{lmax}) for NACA 0012 considered in this study are shown in Figure 7. The figure also shows the tail-rotor blade of a highly loaded blade tip section operating points for the different rotor speeds at three selected altitudes of 0 m, 2000 m and 2400 m. The altitude of 2000 m represents the operating point close to the calculated reference hover ceiling achieved with the base configuration fixed-speed tail-rotor of about 1950 m (for hover OGE, MTOW conditions).

The operating points of this section plotted for the base configuration (100% of N_{ref}) are at the blade stall limits. These points also lie close to the compressibility limits, as they are already operating at around a Mach number of 0.52. The onset of wave-drag rise is already significant at a Mach number of around 0.556. The scope for increasing the rotor speed is thus optimistically only up to 105% of N_{ref} , confirming that compressibility limits area major limitation to operating at higher rotor speeds. At 108% N_{ref} the operating points are above the limits of an imaginary transition limit between blade stall limit and compressibility limits. For a rotor speed of 115% of N_{ref} the operating points of the tip section lie well above the conventional compressibility limits.

For comparison purposes, the blade stall and compressibility limits of DM-H3Tb airfoil developed for a main-rotor tip section[17][18] is reproduced in Figure 7. This airfoil was designed to shift the wave drag rise to higher Mach numbers. The design requirement was however for high helicopter forward speeds and improving the characteristics of advancing blade compressibility limits. For such cases the focus on compressibility limits is operation at low angle of attack and hence lower C_l values at much higher Mach numbers close to 0.8. Use of such airfoils for main-rotor tip section is now commonplace in rotorcraft industry. As can be seen the blade stall limits for DM-H3Tb are also higher due to the cambered design producing higher C_{lmax}. It is noted however that the line representing compressibility limit here is defined at an overall C_d of 0.02 by the authors (as opposed to the drag-divergence from wave drag definition used in this present study). It is unclear if the compressibility limit for the definition used in the present study lies above this line. As such the reference base maximum thrust and hover ceiling would already improve by the use of this airfoil in place of NACA 0012. Assuming this new reference, it is unclear if the hover performance can be significantly improved more than the potential to increase rotor speed to 105% as seen with NACA 0012 airfoil. Further study with such airfoils is recommended.

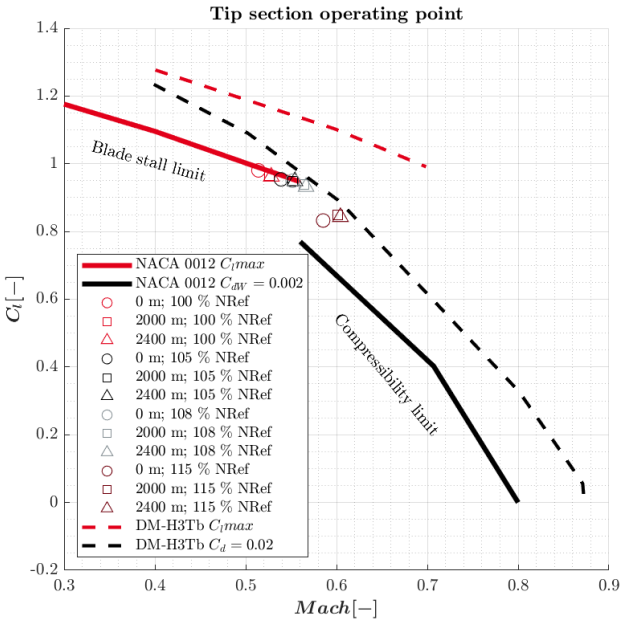

Figure 7 Tail-rotor blade tip section operating point at selected hover altitudes and speeds with airfoil blade stall and compressibility limits.

3.1 Hover ceiling as function of thrust and power balance

The reference power, P_{gbxAv}, is defined as:

(2) $$P_{gbxAv} = \eta_{gbx}\left(\min\left(P_{powerplant} - P_{conspp}, P_{Mgbxlim}\right)\right) - P_{consMgbx}$$

The available aerodynamic power for tail rotor, $P_{TRAvail}$, is given by:

(3) $$P_{TRAvail} = P_{gbxAv} - P_{MR}$$

Where $P_{powerplant}$ is the powerplant maximum all engines operating (AEO) take off power (TOP) at a given altitude, P_{gbxlim} is the gearbox torque limit based power limit, P_{conspp} is an assumed constant value of 30 kW power required for other consumers directly at powerplant such as starter generator, $P_{consMgbx}$ an assumed constant value of 10 kW of power required for other consumers at Main gearbox such as pumps and fans, P_{MR} is the main rotor aerodynamic power and η_{gbx} is the gearbox efficiency.

The value of P_{gbxAv} is taken as 100% reference for Figure 8 which shows the computed main rotor power required for hover OGE with MTOW conditions at different altitudes. For the example helicopter considered, the limiting power at the main gearbox level is actually imposed by the gearbox torque limits and is depicted in Figure 8. The powerplant output reduction due to altitude is above this gearbox limit. Comparing with the thrust balance

shown in Figure 9, it can be said that the base hover ceiling is not limited by the power balance but rather the tail rotor maximum available thrust for the base configuration.

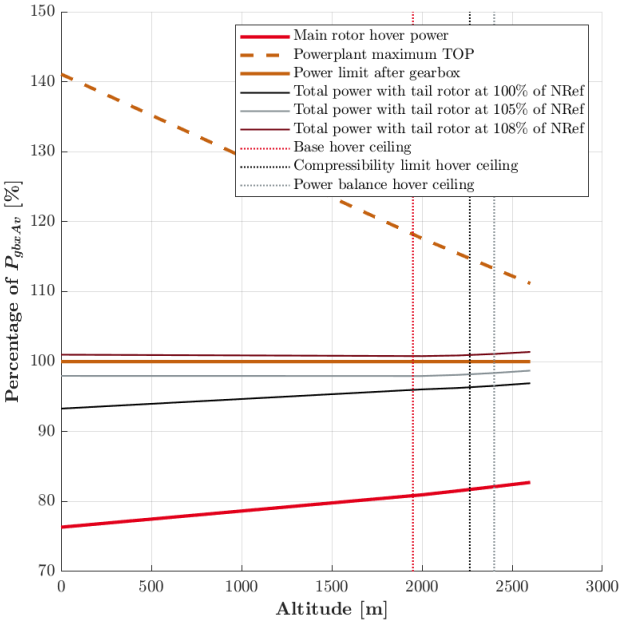

Figure 8 Power balance at main gearbox level for hover OGE at MTOW condition

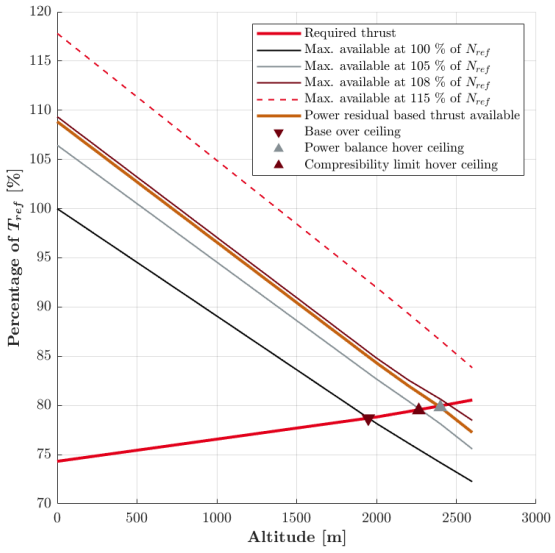

Figure 9 Thrust balance for tail-rotor for hover OGE at MTOW condition

By increasing the operating speed, it can be seen that the hover ceiling can indeed be improved. Based on earlier discussion, with the compressibility effects limiting the usage optimistically up to 105% of N_{ref}, the hover ceiling improves by about 16.2%. However if the increased power demand of operating beyond the compressibility limits are assumed to be capable of being supported, then the speed can be raised to about 107% of N_{ref}, corresponding to the power limit of gearbox at 100% of P_{gbxAv} for which the hover ceiling sees an improvement of up to 23.1%, as represented by the power balance based maximum thrust available.

The results after thrust and power balance limits are summarised in Table 2. For up to the base hover ceiling, the increased speed up to compressibility limits can alternatively be used as additional yaw margin or to increase the rated MTOW for the base hover ceiling.

Table 2 Summary of improvement potential to hover ceiling with variable speed electric tail-rotor for the studied hover OGE at MTOW conditions

	Speed [% of N_{ref}]	Hover ceiling [m]	Improvement [%]
Base	100	1950	-
Compressibility limit	105	2265	16.2
Power balance limit	107	2400	23.1

4. SUMMARY AND CONCLUSION

Potential improvement to hover ceiling limit for helicopters limited by tail-rotor thrust by means of a variable speed electric motor at higher tail-rotor speed operation was identified in literature. The limits to this improvement potential were subsequently explored. To this end tail-rotor blade airfoil section coefficients were calculated on the basis of a 2-D panel method code and transonic small disturbance theory to analyse compressibility effects. A rotor BEM theory model was used to calculate the performance of the tail-rotor. Results presented for an example Helicopter operating in hover OGE with MTOW conditions confirmed that the compressibility effects are a major limitation to increasing tail-rotor operating speed. Optimistic increase is limited to 105% of base operating speed. Thrust and power balance were presented for the tail-rotor and helicopter overall power respectively to determine effective hover ceiling improvement potential compared to base configuration. While with power balance limit a further increase in hover ceiling is possible this is subject to operating beyond compressibility limits. In spite of a small potential to increase tail-rotor operating speed there is considerable hover ceiling improvement potential of up to 16.2% when operating at the optimistic 105% of base operating speed. Further study with airfoils

specifically designed to have wave-drag rise at higher Mach numbers such as those used commonly in main-rotors is recommended.

REFERENCES

[1] Amri, H.; Feil, R.; Hajek, M.; Weigand, M., "Possibilities and difficulties for rotorcraft using variable transmission drive trains", *CEAS Aeronautical Journal*, Vol.7, No.2, 2016, pp. 333–344, doi: 10.1007/s13272-016-0191-6.

[2] Han, D.; Barakos, G. N., "Variable-speed tail rotors for helicopters with variable-speed main rotors", *The Aeronautical Journal*, Vol.121, No.1238, 2017, pp. 433–448, doi: 10.1017/aer.2017.4.

[3] Xie, Jiayi; Guan, Nanxiang; Zhou, Ming; Xie, Zhifeng, "Study on the Mechanism of the Variable-Speed Rotor Affecting Rotor Aerodynamic Performance", *Applied Sciences*, Vol.8, No.7, 2018, pp. 1030, doi: 10.3390/app8071030.

[4] Yin, Jianping; Dummel, Andreas; Falchero, Daniele; Pidd, Mike; Prospathopoulos, John; Visingardi, Antonio; Voutsinas, Spyros G., "Analysis of Tail Rotor noise reduction benefits using HELINOVI aeroacoustic main/tail rotor test and post test prediction results". *32nd European Rotorcraft Forum*, *Maastricht, The Netherlands*, 2006.

[5] Johnson, Wayne, in *Rotorcraft aeromechanics*. Cambridge University Press, Cambridge, 2013. ISBN 9781107028074.

[6] Peterson, Randall L., "Full-Scale Hingeless Rotor Performance and Loads", *NASA Technical Memorandum*. NASA Ames Research Center, Mofett Field, California, 1995.

[7] Drela, Mark, "XFOIL: An analysis and design system for low Reynolds number airfoils", *Low Reynolds number aerodynamics*, Springer, 1989, pp. 1–12.

[8] Murman, E.M.; Bailey, F.R.; Johnson, M.L., "TSFOIL — A Computer Code for Two-Dimensional Transonic Calculations, Including Wind-Tunnel Wall Effects and Wave Drag Evaluation", *NASA SP-347*, March 1975.

[9] Abbott, Ira H.; Doenhoff, Albert E. von, in *Theory of wing sections: including a summary of airfoil data*. Courier Corporation, 2012. ISBN 0486134997.

[10] Holst, Terry L., "Computational fluid dynamics drag prediction: Results from the Viscous Transonic Airfoil Workshop", *NASA Technical Memorandum*, April 1988.

[11] Harris, Charles D., "Two-Dimensional Aerodynamic Characteristics of the NACA 0012 Airfoil in the Langley 8-Foot Transonic Pressure Tunnel", *NASA Technical Memorandum*, April 1981.

[12] Smith, Marilyn J.; Potsdam, Mark; Wong, Tin-Chee; Baeder, James D.; Phanse, Sujeet, "Evaluation of Computational Fluid Dynamics to Determine Two-Dimensional Airfoil Characteristics for Rotorcraft Applications", *Journal of the American Helicopter Society*, Vol.51, No.1, 2006, pp. 70–79.

[13] Scholz, Dieter; Ciornei, Simon, "Mach number, relative thickness, sweep and lift coefficient of the wing - An empirical investigation of parameters and equations". *Deutscher Luft- und Raumfahrtkongress*, *Friedrichshafen, Germany*, 2005.

[14] Gur, Ohad; Mason, William H.; Schetz, Joseph A., "Full-configuration drag estimation", *Journal of Aircraft*, Vol.47, No.4, 2010, pp. 1356–1367.

[15] Ruijgrok, Ger J.J., in *Elements of airplane performance*. VSSD, Delft, The Netherlands, 2009. ISBN 9789065622037.

[16] McCroskey, W.J., "A Critical Assessment of Wind Tunnel Results for the NACA 0012 Airfoil", *NASA Technical Memorandum*. NASA Ames Research Center, October 1987.

[17] Polz, G.; Schimke, D., "New aerodynamic rotor blade design at MBB". *13th European Rotorcraft Forum*, *Arles, France*, 1987.

[18] Horstmann, K.H.; Köster, H.; Polz, G., "Improvement of two blade sections for helicopter rotors". *10th European Rotorcraft Forum*, *The Hauge, The Netherlands*, 1984.